ADVANCED FUNCTIONAL MATERIALS
www.afm-journal.de

Materials Views
www.MaterialsViews.com

A High Energy Density Asymmetric Supercapacitor from Nano-architectured $Ni(OH)_2$/Carbon Nanotube Electrodes

*Zhe Tang, Chun-hua Tang, and Hao Gong**

The demand for advanced energy storage devices such as supercapacitors and lithium-ion batteries has been increasing to meet the application requirements of hybrid vehicles and renewable energy systems. A major limitation of state-of-art supercapacitors lies in their relatively low energy density compared with lithium batteries although they have superior power density and cycle life. Here, we report an additive-free, nano-architectured nickel hydroxide/carbon nanotube ($Ni(OH)_2$/CNT) electrode for high energy density supercapacitors prepared by a facile two-step fabrication method. This $Ni(OH)_2$/CNT electrode consists of a thick layer of conformable $Ni(OH)_2$ nano-flakes on CNT bundles directly grown on Ni foams (NFs) with a very high areal mass loading of 4.85 mg cm^{-2} for $Ni(OH)_2$. Our $Ni(OH)_2$/CNT/NF electrode demonstrates the highest specific capacitance of 3300 F g^{-1} and highest areal capacitance of 16 F cm^{-2}, to the best of our knowledge. An asymmetric supercapacitor using the $Ni(OH)_2$/CNT/NF electrode as the anode assembled with an activated carbon (AC) cathode can achieve a high cell voltage of 1.8 V and an energy density up to 50.6 Wh/kg, over 10 times higher than that of traditional electrochemical double-layer capacitors (EDLCs).

1. Introduction

Electric energy storage devices with high energy storage capacity and fast charge-discharge ability are very important and desirable today as they can find numerous applications in plug-in electric vehicles, back-up power sources, energy storage for wind and solar energy and so forth. Presently the two major areas of advanced energy storage devices are batteries and electrochemical capacitors.[1] Electrochemical capacitors, also known as supercapacitors, are particularly suitable for applications requiring high power density and high charge-discharge rates, such as portable electronic devices, hybrid vehicles and renewable energy systems, due to their much higher power densities than conventional secondary batteries and their long cycle-life (up to 10^4 cycles) and safety tolerance to high rate charge and discharge.[1–4] Currently most commercial supercapacitors are symmetric electric double layer capacitors (EDLCs) based on high surface area carbon materials.[5] They usually have a specific capacitance of about 4 F g^{-1}, a power density of 3–4 kW kg^{-1}, and an energy density of 3–4 Wh kg^{-1} in both aqueous electrolyte and organic electrolyte.[6] A major challenge of using these EDLCs is to boost their energy density to compete with Li-ion batteries for applications in high energy density and high power density power sources.[5–7] To improve the energy density of supercapacitors considerable research efforts have been focusing on developing asymmetric supercapacitors incorporating a EDLC electrode and a non-polarizable electrode using redox-active materials such as transition metal oxides RuO_2, NiO_x, CoO_x, and MnO_2.[8–13] These redox-active materials provide a pronounced improvement in energy density of asymmetric supercapacitors by giving a specific capacitance about 2 to 10 times as large as that of carbon materials as well as a cell voltage higher than ~1 V of EDLCs with aqueous electrolytes.[1] However, the high cost of RuO_2 and the relatively low specific capacitance of NiO_x, CoO_x, and MnO_2 greatly undermine their overall effectiveness for supercapacitor applications.[14–21] Previously several high surface area $Ni(OH)_2$-based electrodes were developed by growing $Ni(OH)_2$ directly onto Ni foams (NFs) to yield a high specific capacitance up to 3125 F g^{-1}; however, its low $Ni(OH)_2$ mass loading ability of only 0.5 mg cm^{-2} considerably limits the areal capacitance down to 1.6 F cm^{-2}.[22,23] To achieve a higher $Ni(OH)_2$ mass loading, $Ni(OH)_2$ nanostructures were deposited onto nanoscaled support materials such as ultrastable Y (USY) zeolite[24] and graphene[25] via wet-chemical precipitation and decontamination processes. The as-deposited $Ni(OH)_2$/support composites were subsequently mixed with conductive agents and organic binders and spread onto NFs through a conventional ink-spread process. It remains one of the most pressing topics in supercapacitor research today to develop a more effective synthesis method for $Ni(OH)_2$-based electrodes with both excellent capacitor-performance and high fabrication-efficiency.[5]

In this study, we report an additive-free, nano-architectured $Ni(OH)_2$/CNT/NF electrode with an ultra-high specific capacitance and a related asymmetric supercapacitor with high energy densities. This nano-architectured $Ni(OH)_2$/CNT/NF electrode is prepared by a facile two-step method, which mainly consists of a direct CVD growth of dense CNT bundles onto NFs followed by a conformal deposition of $Ni(OH)_2$ onto the CNT layers via

Dr. Z. Tang, Ms. C.-h. Tang, Prof. H. Gong
Department of Materials Science and Engineering
National University of Singapore, 117576 Singapore
E-mail: msegongh@nus.edu.sg

DOI: 10.1002/adfm.201102796

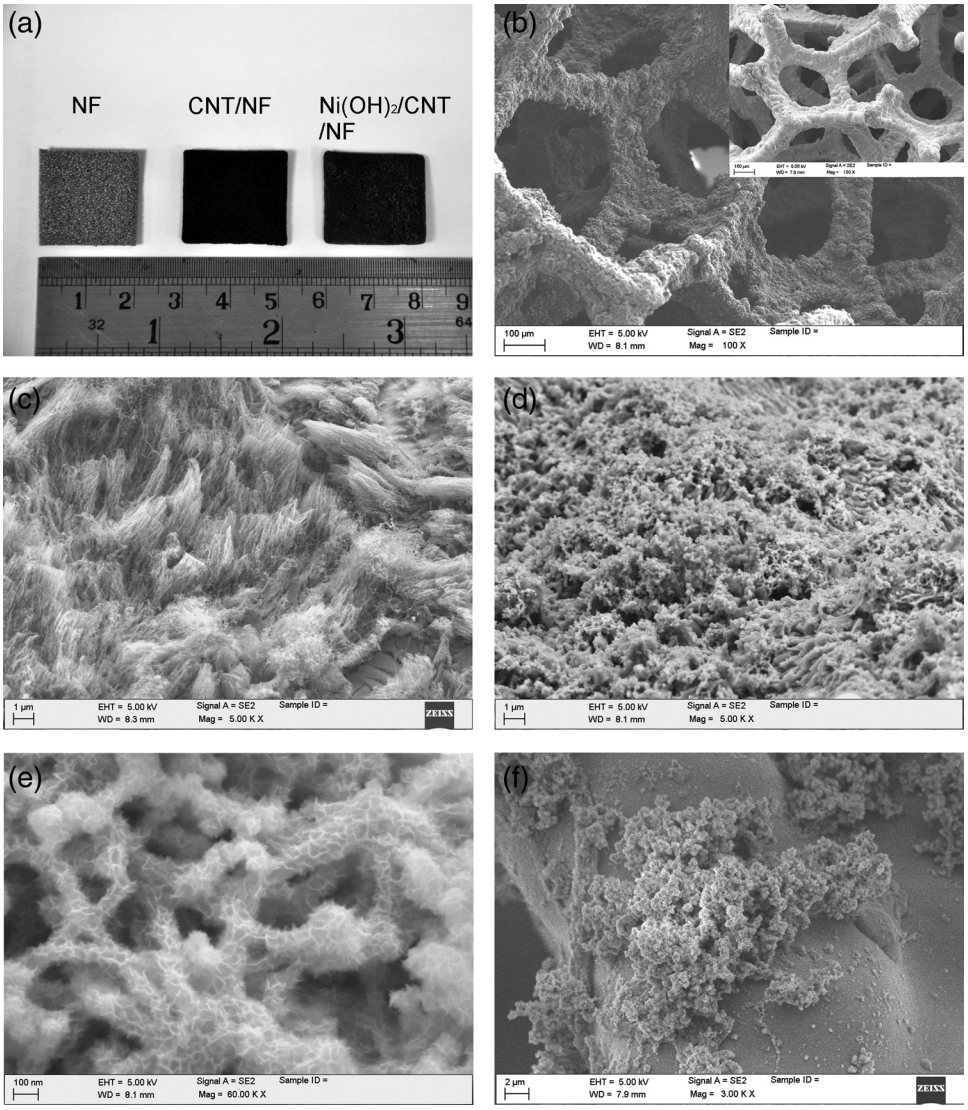

Figure 1. a) photograph of a 2 cm × 2 cm Ni foam, a 2 cm × 2 cm CNT/NF substrate, and a 2 cm × 2 cm $Ni(OH)_2$/CNT/NF electrode, and SEM images of b) NF after CNT growth, inset: pristine NF, c) CNTs grown on NF, d) and e) $Ni(OH)_2$ deposited on CNT/NF, and f) $Ni(OH)_2$ directly deposited on NF without CNT support.

a chemical bath deposition (CBD) process. From a 2 cm × 2 cm monolighic $Ni(OH)_2$/CNT/NF electrode, an exceptionally high specific capacitance of 3300 F g^{-1} was achieved at a high mass loading of 4.85 mg cm^{-2}, giving rise to an area-normalized capacitance up to 16 F cm^{-2}. It allows us to fabricate a thin 4 cm^2 square asymmetric supercapacitor based on a $Ni(OH)_2$/CNT/NF positive electrode and a typical AC negative electrode with a total mass loading of active materials up to about 100 mg. This asymmetric supercapacitor exhibited a significantly elevated cell voltage of 1.8 V and a specific capacitance up to 112.5 F g^{-1} at a charge/discharge current density of 2.5 mA cm^{-2}. The corresponding energy density and power density are 50.6 Wh kg^{-1} and 95 W kg^{-1}, respectively. At a high charge/discharge current density of 50 mA cm^{-2}, its energy density remained at 32.5 Wh kg^{-1} and exhibited excellent cycling stability with only 17% performance loss after 3000 cycles. Furthermore, this 4 cm^2 cell also demonstrated to be able to power up a 3 V mini-fan for about 90 s after a 10s-charging by a AA battery, which substantially indicates its great application potential for commercial viability (see Supporting Information).

2. Results and Discussion

2.1. Structural and Morphological Characterization of $Ni(OH)_2$/CNT/NF Electrodes

The structural and morphological properties of the pristine Ni foam, the CNT-grown NF and the integrated $Ni(OH)_2$/CNT/NF electrode are shown in **Figure 1**. Figure 1a shows a photograph of a pristine Ni foam (NF), a CNT/NF composite

current collector and an integrated $Ni(OH)_2$/CNT/NF electrode, respectively. A uniform growth of CNTs on the porous NF was observed that the NF surface completely turned into dark black. It was also observed that the CNTs were still well-adhered to the NF substrate even after they were subjected to a high speed rotation rinsing at 500 rpm for 3 min, indicating that it was a reliable binder-free integration of the NF and the in-situ grown CNTs to serve as a composite current collector. After $Ni(OH)_2$ deposition, the CNT/NF substrate was covered with a light green lamella, indicating the formation of $Ni(OH)_2$ onto the CNT/NF substrate. Figure 1b shows the SEM images of the NF surface before and after CNT growth. It can be observed that the commercial NF has a 3D network structure with a relatively rough surface (Figure 1b inset). When this NF experienced a CVD process for CNT growth without any additional growth catalysts, its surface roughness was remarkably enhanced by a layer of dense CNT bundles covering its surface as shown in Figure 1b and c. The surface morphology of the $Ni(OH)_2$/CNT/NF electrode is shown in Figure 1d and e. After a direct CBD deposition, the CNT surface was fully covered by nanoscaled $Ni(OH)_2$ flakes showing turbostratic disorder characteristic of a-$Ni(OH)_2$ polycrystals. This unique structure significantly improves the surface area and dispersion of the CBD-deposited $Ni(OH)_2$. It was verified by BET measurement that the surface area of the pristine NF substrate was increased from 0.009 $m^2\ g^{-1}$ to 0.819 $m^2\ g^{-1}$ after coating a thin layer of $Ni(OH)_2$/CNT core/shell nanostructures onto its surface. By contrast, the $Ni(OH)_2$ directly deposited on NF via the same CBD process were densely packed together and showed a rather discrete distribution, leading to a much reduced surface area of about 0.373 $m^2\ g^{-1}$ (Figure 1f). Unlike those segregated $Ni(OH)_2$ particles formed on CNT support in previous studies,[11,25] our $Ni(OH)_2$/CNT/NF electrode fabricated by the two-step method exhibited a fully integrated structure where the Ni foam provides a 3D backbone network and the dense CNT layer serves as a high surface area support for a uniform deposition of nanoscaled $Ni(OH)_2$. This integrated electrode structure substantially guarantees a compact contact for the $Ni(OH)_2$ on the CNT/NF current collector to yield an additive-free electrode with an enhanced $Ni(OH)_2$ loading.

TEM images of the $Ni(OH)_2$ nanostructures on CNT support are shown in **Figure 2**. Instead of forming nanoparticles[11] or nanoflower structures,[13] a gauze-like $Ni(OH)_2$ nano-shell was observed fully covering the CNT surface as shown in Figure 2a. The layered graphitic walls of the CNT support can also be clearly seen underneath the $Ni(OH)_2$ nano-shell as shown in Figure 2a inset. In addition, selected-area electron diffraction (SAED) was performed to investigate the crystalline characteristics of the $Ni(OH)_2$/CNT composite based on the selected area shown in Figure 2a. As shown in Figure 2b, two symmetric diffraction points were clearly seen in the SAED pattern giving a calculated d-spacing of 0.34 nm close to 0.335 nm of graphite layers, which can be correlated to the spacing between the graphitic walls of the CNTs. Moreover, two well-defined rings can also be observed in the SAED pattern, corresponding to the diffraction from the $Ni(OH)_2$ polycrystals. The characteristic crystal planes of the $Ni(OH)_2$ can be indexed as the (110) (111)(200) and (300)(301) planes of a-$Ni(OH)_2$ as shown in Figure 2b,[23] in excellent agreement with their SEM images.

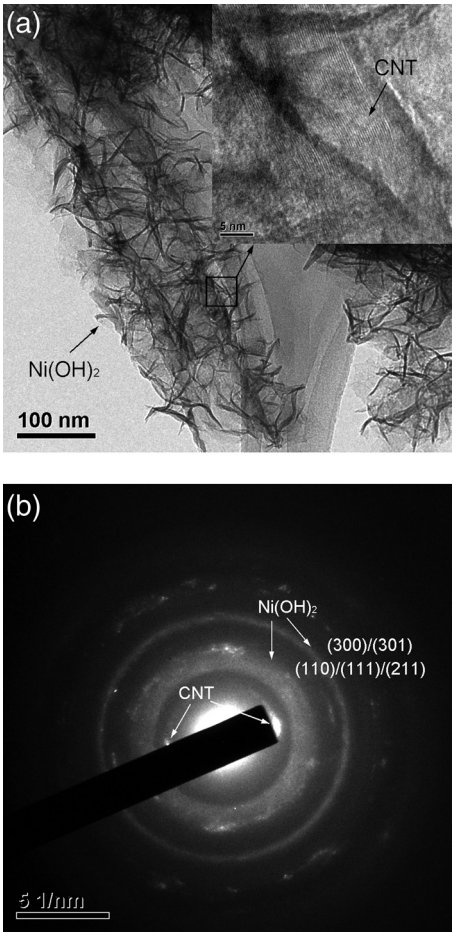

Figure 2. a) TEM image of as-deposited $Ni(OH)_2$/CNT composites, inset: enlarged view of $Ni(OH)_2$/CNT composite showing graphitic walls of the in situ grown CNTs; b) SAED pattern of $Ni(OH)_2$/CNT composites.

2.2. Electrochemical Characterization of $Ni(OH)_2$/CNT/NF Electrode

The electrochemical performance of the integrated $Ni(OH)_2$/CNT/NF electrode was evaluated by CV and galvanostatic charge-discharge measurements in a three-electrode beaker cell with a KOH aqueous electrolyte. **Figure 3**a shows the CV curves of the CNT/NF substrate, the $Ni(OH)_2$/CNT/NF electrode and the $Ni(OH)_2$/NF electrode between a potential window of 0 and 0.4 V at a scan rate of 1 mV/s. The CNT/NF substrate exhibits very low charge storage capability as shown in Figure 3a; whereas a pair of large redox peaks, corresponding to the reversible redox reaction of Ni(II) Ni(III), can be clearly identified in the CV curve of the $Ni(OH)_2$/CNT/NF electrode. This reaction can be illustrated as $Ni(OH)_2 + OH^- \ NiOOH + H_2O + e^-$, which involves the intercalation and deintercalation of protons.[26] This result clearly indicates that the charge storage mechanism of the $Ni(OH)_2$/CNT/NF electrode is mainly ascribed to the pseudo-capacitance from the Faradaic processes of the high surface area $Ni(OH)_2$ nano-flakes. In addition, the anodic and cathodic peaks showed a highly symmetric characteristics, suggesting a high redox reversibility of the CBD-deposited

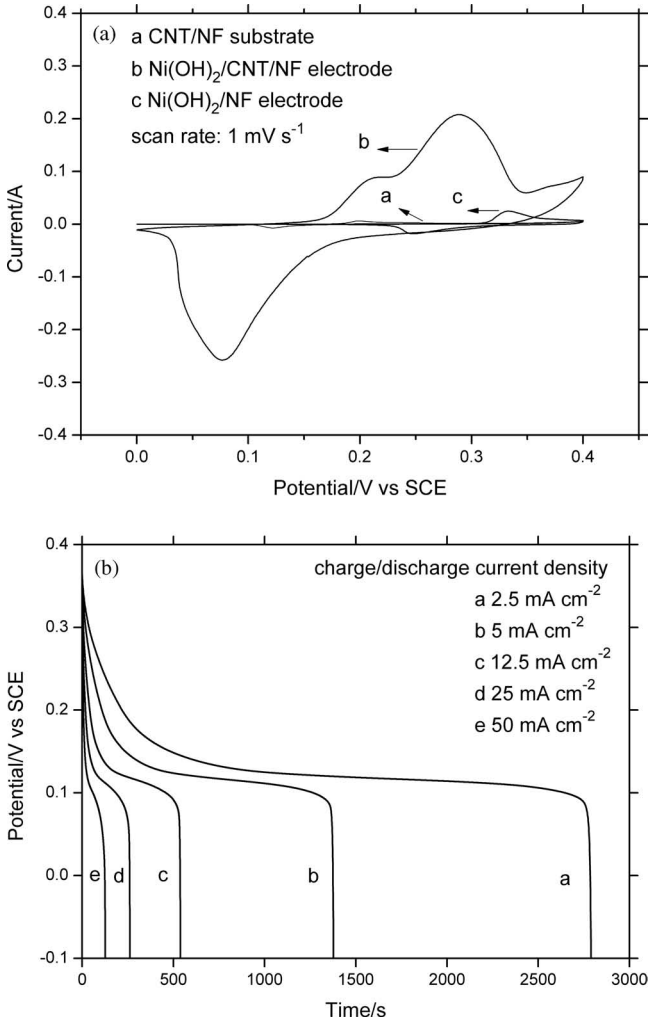

Figure 3. a) CV curves of CNT/NF, $Ni(OH)_2$/CNT/NF and $Ni(OH)_2$/NF electrodes at a scan rate of 1 mV s^{-1}. b) Galvaatic discharge curves of $Ni(OH)_2$/CNT/NF electrode at discharge current densities of 2.5, 5, 12.5, 25 and 50 mA cm^{-2}, respectively.

$Ni(OH)_2$ nano-flakes. By contrast, the CV curve of the $Ni(OH)_2$/NF electrode without an integrated CNT layer showed a much reduced redox peak current compared with the $Ni(OH)_2$/CNT/NF electrode. From the CV results, the specific capacitance and area-normalized capacitance of the $Ni(OH)_2$/CNT/NF electrode, excluding the contribution from the CNT/NF substrate, were calculated to be about 3300 F g^{-1} and 16 F cm^{-2} (based on the mass of $Ni(OH)_2$). They are the highest values, to the best of our knowledge, among the reported supercapacitor materials in previous studies as shown in **Table 1**.[22–25,27] The $Ni(OH)_2$/NF electrode without CNT support prepared by direct $Ni(OH)_2$ deposition onto NFs exhibited a lower specific capacitance of 2820 F g^{-1} and a considerably reduced mass loading ability of 0.25 mg cm^{-2}. The ultra-high specific capacitance of the $Ni(OH)_2$/CNT/NF electrode can be mainly attributed to the high utilization of the well-dispersed $Ni(OH)_2$ nano-flakes on the high surface area CNT/NF current collector. Moreover, the highly conductive CNT and the turbostratic disorder characteristic of

Table 1. Areal loading and specific capacitance of $Ni(OH)_2$/CNT/NF and $Ni(OH)_2$/NF electrodes in this study, compared with some $Ni(OH)_2$-based electrodes reported in previous literature.

Electrode Structure	Electrode Fabrication Method	Specific Capacitance (F g^{-1})	Areal $Ni(OH)_2$ Loading (mg cm^{-2})	Area-normalized Capacitance (F cm^{-2})
$Ni(OH)_2$/CNT/NF (this study)	CVD + CBD	3300	4.85	16
$Ni(OH)_2$/NF (this study)	CBD	2820	0.25	0.7
$Ni(OH)_2$/NF (ref. 23)	CBD	2200	1.92	4.2
$Ni(OH)_2$/NF (ref. 22)	Electrodeposition	3152	0.5	1.6
$Ni(OH)_2$/USY (ref. 24)	Chemical precipitation	1740	3.35	5.8
$Ni(OH)_2$/Graphene (ref. 25)	Hydrolysis + Hydrothermal	1335	0.7	0.9

a-$Ni(OH)_2$ structure arising from intercalation of anions and water molecules further enhance the active surface area and carrier transport and facilitates the surface-dependant Faradaic processes.[28,29] Therefore the superior electrochemical performance of our $Ni(OH)_2$/CNT/NF electrode can be accounted for its highly disordered a-$Ni(OH)_2$ structure on conducting CNT and extensively nano-architectured morphology. Comparing previously developed $Ni(OH)_2$-based electrodes, our $Ni(OH)_2$/CNT/NF electrode also provides a notably enhanced areal $Ni(OH)_2$ loading, yielding a much higher overall capacity of the electrode. This result further confirms that the integrated CNT/NF current collector can considerably improve the mass load for $Ni(OH)_2$ deposition while ensure a high utilization of the CBD-deposited $Ni(OH)_2$ nanoflakes.

A series of charge/discharge measurements were performed on the $Ni(OH)_2$/CNT/NF electrode at various charge/discharge currents of 10, 20, 50, 100 and 200 mA (corresponding to 2.5, 5, 12.5, 25 and 50 mA/cm^2). The discharge curves of the $Ni(OH)_2$/CNT/NF electrode at different charge/discharge currents are shown in Figure 3b. Unlike the linear characteristic of EDLC electrodes, the discharge curves of the $Ni(OH)_2$/CNT/NF electrode exhibited a typical pseudocapacitive behavior, which agrees very well with its CV results. By calculating its specific capacitance at different discharge currents, we found a visibly lower capacitance loss of 33% of the $Ni(OH)_2$/CNT/NF electrode at a high charge/discharge current of 10 A g^{-1} (50 mA cm^{-2}), in contrast to 68% loss of the $Ni(OH)_2$/CNT-based electrode at 12 A g^{-1} (6 mA cm^{-2}) reported previously.[22] It clearly indicates that our $Ni(OH)_2$/CNT/NF electrode can provide a more reliable capacitive performance at high rates for high power applications. Previously, $Ni(OH)_2$ was usually transformed into NiO_x due to the poor high rate capability of $Ni(OH)_2$ despite of its higher specific capacitance than NiO_x.[13,25,26] By contrast, such transformation is exempted by using the $Ni(OH)_2$/CNT/NF electrode to provide both a high specific capacitance and a high rate capacity. This improvement mainly arises from the compact electrode structure where the active $Ni(OH)_2$ nanostructures are effectively incorporated onto the highly conductive CNT/NF current collector.

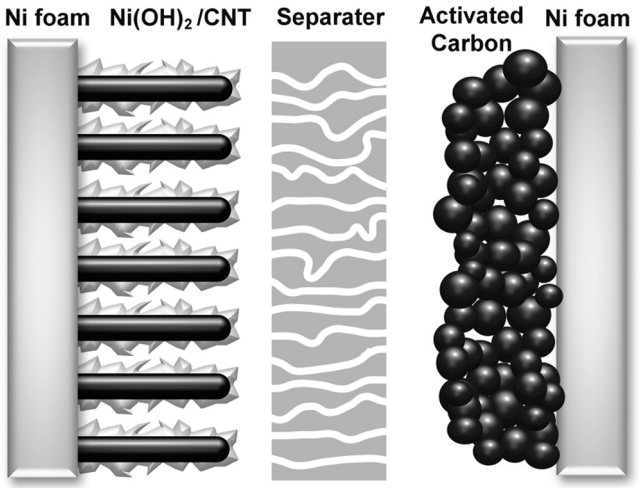

Figure 4. Illustration of $Ni(OH)_2$/CNT-AC Asymmetric Supercapacitor in 6 M KOH electrolyte.

2.3. Electrochemical Characterization of $Ni(OH)_2$/CNT-AC Asymmetric Supercapacitor

To evaluate the capacitive performance of the $Ni(OH)_2$/CNT/NF electrode in a full cell set-up, a 2 cm × 2 cm $Ni(OH)_2$/CNT-AC-based asymmetric supercapacitor was developed in our study using a $Ni(OH)_2$/CNT/NF-based anode and an AC-based cathode, as illustrated in **Figure 4**. The charge/discharge process of the asymmetric supercapacitor can be schematically demonstrated as $Ni(OH)_2 + OH^-$ $NiOOH + H_2O + e^-$ at the $Ni(OH)_2$/CNT positive electrode and $C + KOH$ $CK^+ + OH^-$ at the AC negative electrode.[30] The total mass of the active materials on the anode and cathode were 20 and 80 mg, close to the ideal mass ratio 4.29 to obtain a maximum energy density proposed by Zheng.[31] The AC-based electrode exhibited a specific capacitance of 120 F g^{-1} at a discharge current of 50 mA cm^{-2}, comparable to that of the state-of-the-art AC-based electrodes (see supporting information).[11] **Figure 5**a shows the CV curve of the $Ni(OH)_2$/CNT-AC-based asymmetric supercapacitor at a scan rate of 5 mV s^{-2} in a KOH electrolyte. Unlike the sharp redox peaks observed in the CV curve of the $Ni(OH)_2$/CNT/NF electrode, the asymmetric supercapacitor showed a rectangle-like CV curve in a large potential range from 0 to 1.8 V, indicating a typical capacitor behavior as EDLCs or RuO_2. This behavior was rarely seen in previous studies on $Ni(OH)_2$-based asymmetric supercapacitors.[11,13] Moreover, the cell voltage of the $Ni(OH)_2$/CNT-AC-based asymmetric supercapacitor was increased to 1.8 V, which is almost twice as that of conventional AC-based supercapacitors in aqueous electrolytes (~1 V).[1] This is a critical factor to improve its energy density property considering that the cell energy density is given by $E = 1/2\ CV^2$, where C represents the specific capacitance and V is the cell voltage[1]. Furthermore, galvanostatic discharge curves at various charge/discharge current densities are shown in Figure 5(b). In contrast to the battery-like discharge curves of the $Ni(OH)_2$/CNT/NF electrode in Figure 3b, the discharge curves of the $Ni(OH)_2$/CNT-AC asymmetric supercapacitor showed nearly a linear variation with cell potential, further indicating its capacitor-like behavior. The calculated specific capacitances based on the total mass of the active materials (c.a. 100 mg) at 2.5, 5, 12.5, 25 and 50 mA cm^{-2} are 112.5, 110.6, 105.5, 92.8 and 72.2 F g^{-1}. It should be noted that the specific capacitance of the full cell is limited by that of the AC-based cathode (~120 F g^{-1}); nevertheless, it is significantly enhanced by the ultra-high pseudo-capacitance of the $Ni(OH)_2$/CNT/NF electrode to about 3-fold larger than conventional AC-based symmetric capacitors (~20 F g^{-1}).[4] The corresponding energy density and power density at 2.5 mA cm^{-2} were 50.6 Wh kg^{-1} and 95 W kg^{-1}, respectively. At a high discharge current of 50 mA cm^{-2}, the energy density remained at 32.5 Wh kg^{-1} at a power density of 1800 W kg^{-1}. The superior energy density property of our asymmetric supercapacitor can be attributed to both its high specific capacitance and its much elevated cell voltage of 1.8 V in the aqueous electrolyte. With a high energy density and an enhanced mass loading, our asymmetric supercapacitor demonstrated the ability to be charged by a AA battery for only 10 s and discharged to power up a 3 V mini-fan for about 90 s (see Supporting Information).

Figure 5c presents the Ragone plot (energy density vs. power density) of the $Ni(OH)_2$/CNT-AC asymmetric supercapacitor derived from its discharge curves at various charge/discharge currents. In view of the low energy density of state-of-art AC-based EDLCs,[4] the superior energy density property of our asymmetric supercapacitor considerably boosts its application potential to replace traditional EDLCs in advanced energy storage devices and possibly find applications where Li-ion batteries are dominant. The cycling stability of the $Ni(OH)_2$/CNT-AC asymmetric supercapacitor was further investigated by means of galvanostatic charge/discharge cycling between 0 and 1.8 V at a high current density of 50 mA cm^{-2} (200 mA). A total number of 3000 cycles was continuously performed and the specific capacitance variation of the asymmetric capacitor along the cycling test was normalized as shown in Figure 5d. A total capacitance loss of 17% was observed after the cell experienced 3000 charge/discharge cycles, which may probably be due to the loosening of the AC layer from the NF current collector at the cathode. This speculation was confirmed by pressing the cathode after the cycling test and the capacitance loss was reduced to 5%. Comparing to the 48% capacitance loss of the $Ni(OH)_2$/NF-based electrode after only 300 charge/discharge cycles reported previously,[22] our $Ni(OH)_2$/CNT-AC asymmetric supercapacitor demonstrates an excellent cycling stability after 3000 charge/discharge cycles at a high charge-discharge rate. It is very likely that its capacitance loss can be further improved when its electrodes are assembled in a capsulation cell to prevent loosening or flaking off of the active materials.

3. Conclusions

In summary, a nano-architectured $Ni(OH)_2$/CNT/NF electrode with high capacitance has been efficiently fabricated via a two-step process, and a relevant high energy density asymmetric supercapacitor has been achieved. The two-step fabrication process allows us to directly grow CNT layers onto Ni foams for a conformal deposition of $Ni(OH)_2$ nano-flakes onto the CNT/NF composite current collectors. The as-deposited $Ni(OH)_2$ showed a nanoscaled gauze-like structure and a uniform dispersion on

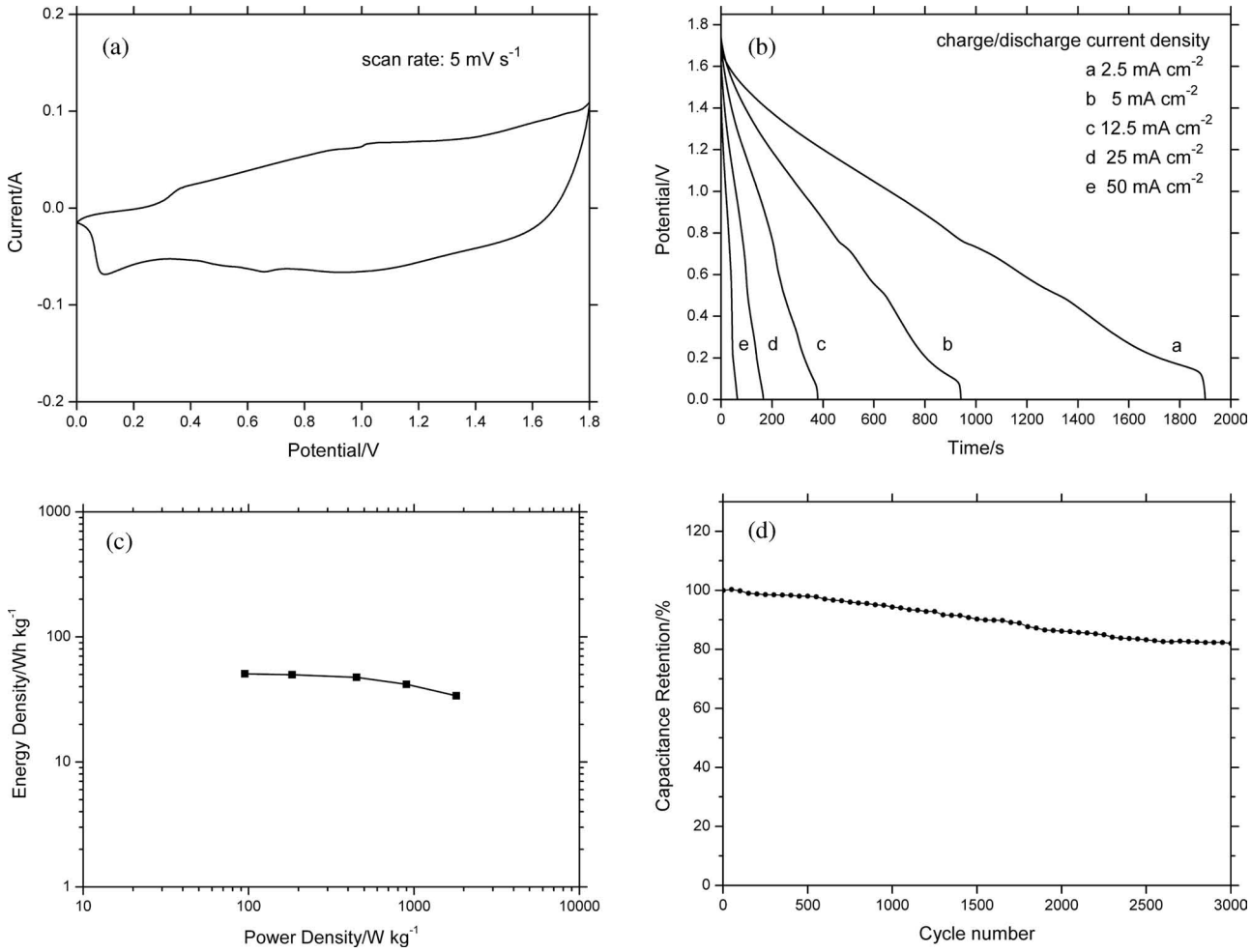

Figure 5. a) CV of $Ni(OH)_2$/CNT-based asymmetric supercapacitor between 0 and 1.8 V at a scan rate: 5 mV s^{-1}. b) Discharge curves of $Ni(OH)_2$/CNT-based asymmetric supercapacitor at discharge current densities of 2.5, 5, 12.5, 25 and 50 mA cm^{-2}, respectively. c) Ragone plot (energy density vs. power density) of $Ni(OH)_2$/CNT-AC asymmetric supercapacitor. d) Cycle life of $Ni(OH)_2$/CNT-AC asymmetric supercapacitor at a charge/discharge current density of 50 mA cm^{-2} for 3000 cycles.

the CNT surface. This integrated electrode structure remarkably enhanced the mass loading of $Ni(OH)_2$ while maintaining a high utilization of the $Ni(OH)_2$ nanostructures. Compared with previously developed $Ni(OH)_2$-based electrodes, our nano-architectured $Ni(OH)_2$/CNT/NF electrode exhibited the highest specific capacitance of 3300 F/g at a high $Ni(OH)_2$ loading of 4.85 mg cm^{-2}. It paves the way for using pseudo-capacitance materials to yield additive-free, high-conductivity and high-capacitance electrodes for asymmetric supercapacitor applications. An asymmetric supercapacitor based on this $Ni(OH)_2$/CNT/NF electrode has also been developed in this study and it exhibits a high energy density comparable to that of Li-ion batteries at a high power density as that of supercapacitors. The $Ni(OH)_2$/CNT-AC asymmetric supercapacitor has demonstrated a great application potential for its superior capacitive performance and cycling stability. Our future research work will concentrate on developing scaled-up supercapacitor prototypes using the integrated electrodes in non-aqueous electrolytes to further boost their energy densities. Moreover, new cathode materials will be developed to replace conventional activated carbon at cathode, which is the limiting factor for the specific capacitance of our $Ni(OH)_2$/CNT-AC asymmetric supercapacitor. In addition, the two-step fabrication process also provides numerous application versatilities to incorporate transition metal oxides and hybrid pseudo-capacitive materials onto the nanostructured CNT/NF current collectors for electrodes in various energy storage devices.

4. Experimental Section

In the first step of preparing the $Ni(OH)_2$/CNT/NF electrode, CNTs were directly grown onto Ni foams via a thermal chemical vapor deposition (CVD) process. In a typical CVD process of in situ CNT growth, several 2 cm × 2 cm Ni foams without additional catalysts were heated up in a tube furnace at 750° in carbon feedstock gas C_2H_4. In the second step, a chemical bath deposition (CBD) process was carried out to deposit $Ni(OH)_2$ nanostructures onto the as-grown CNT/NF current collectors. The CNT/NF substrates were immerged into a mixture solution of aqueous ammonia with nickel sulfates and potassium persulfates. The $Ni(OH)_2$ deposition was performed at room temperature after which the $Ni(OH)_2$-grown CNT/NF substrates were dried at 120° before

electrochemical testing. The mass loading of the CBD-deposited $Ni(OH)_2$ on CNT/NF substrates was determined by the weight difference of the total electrode mass before and after the CBD process. The microstructure was characterized by both scanning electron microscopy (SEM, JOEL JSM-6700F) and transmission electron microscopy (TEM, JOEL JEM-2010).

The asymmetric supercapacitor was developed based on a $Ni(OH)_2$/CNT/NF positive electrode and a AC-based negative electrode. The AC-based negative electrode was prepared by mixing 95 wt% activated carbon (Black Pearl 2000, Cabot) and 5 wt% PTFE and spreading the mixture on to a 2 cm × 2 cm Ni foam. Both the positive and the negative electrodes were pressed individually and assembled into an asymmetric supercapacitor. A series of electrochemical tests including cyclic voltammetry (CV) and galvanostatic charge-discharge measurement were performed in a three-electrode compartment with a Solartron Electrochemical System SI 1296. A KOH solution was used as the electrolyte and a saturated calomel electrode (SCE) was used as the reference electrode and a 2 cm^2 Pt foil as the counter electrode. An example embodiment of this asymmetric supercapacitor was also demonstrated with an AA battery as the charge source and a 3 V mini-fan as the discharge load, which was shown in the supporting information.

(CDC JCPDS#22-0444 contains the supplementary crystallographic data for this paper. These data can be obtained free of charge from The Cambridge Crystallographic Data Centre via www.ccdc.cam.ac.uk/data_request/cif.)

Supporting Information

Supporting Information is available from the Wiley Online Library or from the author.

Acknowledgements

A-STAR SERC Grant 0721330044 (R284000067592) and MoE AcRF Tier 1 grant R284-000-071-112 supports are appreciated.

Received: November 19, 2011
Revised: December 15, 2011
Published online: January 19, 2012

[1] B. E. Conway, *Electrochemical Supercapacitors: Scientific Fundamentals and Technological Applications*, Kluwer Academic/Plenum: New York **1999**.
[2] M. Winter, R. J. Brodd, *Chem. Rev* **2004**, *104*, 4245.
[3] A. S. Arico, P. Bruce, B. Scrosati, J. Tarascon, W. V. Schalkwijk, *Nat. Mater.* **2005**, *4*, 366.
[4] Y. G. Guo, J. S. Hu, L. J. Wan, *Adv. Mater.* **2008**, *20*, 2878.
[5] P. Simon, Y. Gogotsi, *Nat. Mater.* **2008**, *7*, 845.
[6] P. C. Chen, G. Shen, Y. Shi, H. Chen, C. Zhou, *ACS Nano* **2010**, *4*, 4403.
[7] J. M. Tarascon, M. Armand, *Nature* **2001**, *414*, 359.
[8] G. G. Amatucci, F. Badway, A. Du Pasquier, T. J. Zheng, *Electrochem. Soc.* **2001**, *148*, A930.
[9] A. Du Pasquier, I. Plitz, J. Gural, S. Menocal, G. Amatucci, *J. Power Sources* **2003**, *113*, 62.
[10] A. Du Pasquier, A. Laforgue, P. Simon, *J. Power Sources* **2004**, *125*, 95.
[11] Y. G. Wang, L. Yu, Y. Y. Xia, *J. Electrochem. Soc.* **2006**, *153*, A743.
[12] D. W. Wang, F. Li, H. M. Cheng, *J. Power Sources* **2008**, *185*, 1563.
[13] H. Inoue, Y. Namba, E. Higuchi, *J. Power Sources* **2010**, *195*, 6239.
[14] J. P. Zheng, P. J. Cygan, T. R. Zow, *J. Electrochem. Soc.* **1995**, *142*, 2699.
[15] Y. G. Wang, Z. D. Wang, Y. Y. Xia, *Electrochim. Acta* **2005**, *50*, 5641.
[16] C. Lin, J. A. Ritter, B. N. Popov, *Electrochem. Soc.* **1998**, *145*, 4097.
[17] L. B. Kong, J. W. Lang, M. Liu, Y. C. Luo, L. Kang, *J. Power Sources* **2009**, *194*, 1194.
[18] S. C. Pang, M. A. Anderson, T. W. Chapman, *J. Electrochem. Soc.* **2000**, *147*, 444.
[19] K. C. Liu, M. A. Anderson, *J. Electrochem. Soc.* **1996**, *143*, 124.
[20] V. Srinivasan, J. W. Weidner, *J. Electrochem. Soc.* **1997**, *144*, L210.
[21] K. W. Nam, K. B. Kim, *J. Electrochem. Soc.* **2002**, *149*, A346.
[22] G. W. Yang, C. L. Xu, H. L. Li, *Chem. Commun.* **2008**, *48*, 6537.
[23] G. X. Hu, C. X. Li, H. Gong, *J. Power Sources* **2010**, *195*, 6977.
[24] L. Cao, L. B. Kong, Y. Y. Liang, H. L. Li, *Chem. Commun.* **2004**, *14*, 1646.
[25] P. Lin, Q. J. She, B. L. Hong, X. J. Liu, Y. N. Shi, Z. Shi, M. S. Zheng, Q. F. Dong, *J. Electrochem. Soc.* **2010**, *157*, A818.
[26] K. W. Nam, K. H. Kim, E. S. Lee, W. S. Yoon, X. Q. Yang, K. B. Ki, *J. Power Sources* **2008**, *182*, 642.
[27] L. Cao, F. Xu, Y. Y. Liang, H. L. Li, *Adv. Mater.* **2004**, *16*, 1853.
[28] G. H. A. Therese, P. V. Kamath, J. Gopalakrishnan, *J. Solid State Chem.* **1997**, *128*, 38.
[29] F. Portemer, A. Delahaye-Vidal, M. Figlarz, *J. Electrochem. Soc.* **1992**, *139*, 671.
[30] N. W. Duffy, W. Baldsing, A. G. Pandolfo, *Electrochim. Acta* **2008**, *54*, 535.
[31] J. P. Zheng, *J. Electrochem. Soc.* **2003**, *150*, A484.